frontiers in Materials

ORIGINAL RESEARCH
published: 13 October 2021
doi: 10.3389/fmats.2021.715104

Improving the *in vitro* Degradation, Mechanical and Biological Properties of AZ91-3Ca Mg Alloy via Hydrothermal Calcium Phosphate Coatings

Asif Ali[1], Fakhera Ikram[1], Farasat Iqbal[1]†, Hira Fatima[1], Azra Mehmood[2], Maruf Yinka Kolawole[3], Aqif Anwar Chaudhry[1], Saadat Anwar Siddiqi[1] and Ihtesham Ur Rehman[4]*

[1]Interdisciplinary Research Centre in Biomedical Materials, COMSATS University Islamabad, Lahore Campus, Lahore, Pakistan, [2]Centre of Excellence in Molecular Biology (CEMB), University of the Punjab, Lahore, Pakistan, [3]Mechanical Engineering Department, Kwara State University, Ilorin, Nigeria, [4]Bioengineering, Engineering Department, Lancaster University, City of Lancaster, United Kingdom

OPEN ACCESS

Edited by:
Oliver Goerke,
Technical University of Berlin, Germany

Reviewed by:
Lei Sui,
Tianjin Medical University, China
Andre D. R. Silva,
Brazilian Air Force Academy, Brazil

***Correspondence:**
Farasat Iqbal
farasatiqbal@cuilahore.edu.pk

†Present address:
Farasat Iqbal,
Interdisciplinary Research Centre in Biomedical Materials, Lahore Campus, COMSATS University Islamabad, Lahore, Pakistan

Specialty section:
This article was submitted to Biomaterials, a section of the journal Frontiers in Materials

Received: 26 May 2021
Accepted: 31 August 2021
Published: 13 October 2021

Citation:
Ali A, Ikram F, Iqbal F, Fatima H, Mehmood A, Kolawole MY, Chaudhry AA, Siddiqi SA and Rehman IU (2021) Improving the in vitro *Degradation, Mechanical and Biological Properties of AZ91-3Ca Mg Alloy via Hydrothermal Calcium Phosphate Coatings. Front. Mater. 8:715104. doi: 10.3389/fmats.2021.715104*

For many years, calcium phosphate coatings to tailor the degradation behavior of magnesium and magnesium-based alloys for orthopaedic applications have received lots of research attention. However, prolong degradation behavior, its effect on biological and mechanical properties as well as osteoblastic response to single-step hydrothermally deposited calcium phosphate coatings remain poorly documented. In this study, Alamar blue assay, cell attachment, live/dead assay, and qRT-PCR were done to study the biological response of the coatings. Furthermore, immersion testing in SBF for 28 days and compression testing of the degraded samples were carried out to examine the degradation behavior and its effect on mechanical properties. The results indicated that coatings have a significant influence on both the substrate performance and structural integrity of coated AZ91-3Ca alloy. Immersion test revealed that coating deposited at pH 7, 100°C (CP7100) improves the hydrogen evolution rate by 65% and the degradation rate by 60%. As the degradation performance of coated samples improves so does the mechanical strength. CP7100 samples successfully retained 90% of their compressive strength after 14 days of immersion while bare AZ91-3Ca alloy lost its mechanical integrity. Furthermore, biological studies show that cells are happily proliferating, differentiating, and adhering to the coating surfaces, which indicates, improved osteointegration and osteogenesis with no sign of alkaline poisoning. qRT-PCR results showed that calcium phosphate coatings enhanced the mRNA levels for *RUNX2*, *Col1A*, and *ALP* that may exhibit a speedy bone recovery. Thus, calcium phosphate coatings produced via a single-step hydrothermal method improve the degradation behavior, mechanical integrity and stimulate the differentiation of osteoblast lining. This leads toward faster bone regeneration, which shows a great potential of these coatings to be used on degradable implants as a bioactive protective layer.

Keywords: calcium phosphate, biodegradable magnesium, bioactive coatings, Az91, osteogenesis, MC3T3-E1

INTRODUCTION

Magnesium is an exceptionally lightweight metal with excellent mechanical properties. It has a Young's modulus and yield strength closer to that of natural bone which decreases stress shielding effect hence, offers adequate stress transfer to fractured bone (Staiger et al., 2006; Gao et al., 2017; Haghshenas, 2017; Radha and Sreekanth, 2017). In a physiological environment, magnesium metal reacts with surrounding water to develop a mild protective layer of magnesium hydroxide. The chloride ions present in the physiological environment react with $Mg(OH)_2$ layer and convert it into soluble magnesium chloride with evolution of hydrogen gas. This exposes the magnesium substrate to be further attacked by surrounding water and faster corrosion followed by abrupt hydrogen evolution (Staiger et al., 2006; Brar et al., 2009). This abrupt corrosion and hydrogen evolution pose a serious threat to host tissue as well as to the stability of the magnesium-based implant. This causes cell death and generation of gas cavities in host tissues resulting in detachment of cells from the implant surface and premature loss of mechanical integrity before tissue healing (Noviana et al., 2016). Abrupt hydrogen evolution also increases the localized pH, which harshly affects the biological process as the alkalization increases rapidly around the implant surroundings (Song, 2007; Lorenz et al., 2009; Schumacher et al., 2014). These shortcomings are currently a limiting factor for magnesium-based alloys to be safely used in load-bearing orthopaedic applications.

To overcome this rapid corrosion, various strategies have been deployed including developing alloys with low degradation rates, using bioactive coatings and surface treatments to retard the corrosion rates in physiological conditions. Alloying with rare earth elements improves the corrosion resistance but released ions may have adverse effects and toxicity especially in the case of children (Pichler et al., 2014). In addition, zirconium, that is used as a grain refiner for strength enhancement in magnesium and its alloys has associated health challenges such as nasopharyngeal, breast, lung, and liver cancer (Song, 2007). Besides Zr, some other elements like cerium, praseodymium, and lutetium also show toxic effects (Song, 2007; Brar et al., 2009). To overcome these complex challenges, biocompatible and bioactive coatings have been extensively reported to provide a viable solution (Radha and Sreekanth, 2017). Bioactive coatings offer a better route to decrease the corrosion rate by providing a physical corrosion barrier as well as a friendly interface for cell attachment and proliferation (Hornberger et al., 2012; Rahim et al., 2017).

Coatings comprising of calcium phosphate (D'antonio et al., 2004) are reported as nontoxic, chemically identical to the composition of the natural bone, and adhesive to the surrounding tissues. They also provide support in bone growth and apatite formation when exposed to the simulated body fluid. *In vitro* cytocompatibility, *in vivo* osteoconductivity, and osteogenesis improve significantly by calcium phosphate coatings when used on magnesium and its alloys (Gray-Munro and Strong, 2009; Horynová et al., 2019). Surface energy and protein adsorption increased on the coated surface with positively charged corroded ions that provide support to the mature bone cells and stimulate the differentiation of osteoblast linings (Narayanan et al., 2008). *In vitro* and clinical studies also reported improved cell differentiation, their growth, and attachment on the calcium phosphate-coated substrate (Shadanbaz and Dias, 2012). The released calcium ions as a degradation product of coating serve as active sites for the adhesion and proliferation of osteoblast and bone cells (Narayanan et al., 2008).

The apatite layer is responsible for better initial adhesion and cells proliferation. It is reported (Keim et al., 2011) that apatite coating minimizes the corrosion rate by 60% as compared to pure Mg as this will greatly reduce the risk of alkaline poising resulting in improved cell proliferation and adhesion. Better adhesion of the cells and stability of the implanted material lead towards proper osteointegration and fixation of the fracture. Surface roughness induced by calcium phosphate coatings enhances the cell adhesion, which results in the slow degradation of the substrate and an improved mechanical fixation of the implants with host tissue. Cell adhesion increases as surface roughness increases which slow down the biodegradation process by limiting the access of corrosive medium to the substrate surface thus providing maximum mechanical stability to fracture bone area (Biggs et al., 2007).

Several techniques have been employed to deposit calcium phosphate (D'antonio et al., 2004) coatings on magnesium-based alloys. However, to minimize product cost and environmental load, a single-step hydrothermal method seems a preferable option. The calcium phosphate coatings using this method has been investigated and reported by many authors utilizing different deposition parameters (Hiromoto and Yamamoto, 2009; Hiromoto and Tomozawa, 2010; Asl et al., 2014; Asl et al., 2015a; Asl et al., 2015b; Ali et al., 2019). In addition, investigation on the effect of process parameters of single-step hydrothermal CaP coating performance such as biological response, prolonged degradation behavior, and its effect on the mechanical strength of magnesium alloy is rarely found in the literature. To the best of our knowledge, this is the first study investigating the biological responses, prolonged degradation behavior and its effect on the mechanical strength of CaP coated magnesium alloys for potential orthopaedic application. Therefore, the goal of the present study is to understand the prolonged degradation behavior, its effect on mechanical properties as well as the detailed biological response of calcium phosphate coated magnesium alloys for potential orthopaedic application.

MATERIALS AND METHODS

AZ91-3Ca magnesium alloy, generously provided by the Institute of General Materials Properties, FAU Erlangen Nuremberg, Germany, used as a substrate. Diammonium hydrogen phosphate ($(NH_4)_2HPO_4$) and calcium nitrate ($Ca(NO_3)_2.4H_2O$) were used as coating precursors. Ammonium hydroxide (NH_4OH) and hydrochloric acid (HCl) were used to adjust the solution pH as required. The detailed single-step hydrothermal coating process has been reported in our previous work (Ali et al., 2019). Briefly, a solution containing

TABLE 1 | Order and amount of reagents used for the preparation of 1000 ml SBF.

Order	Regent	Amount
1	NaCl	8.035 g
2	$NaHCO_3$	0.355 g
3	KCL	0.225 g
4	$K_2HPO_4.\ 3H_2O$	0.231 g
5	$MgCl_2.\ 6H_2O$	0.311 g
6	1.0 M-HCl	39 ml
7	$CaCl_2$	0.292 g
8	Na_2SO_4	0.072 g
9	Tris	6.118 g
10	1.0 M-HCl	0–5 ml

1 M calcium nitrate and 0.6 M diammonium hydrogen phosphate was prepared, and a 10 ml/cm^2 solution to sample surface area ratio was used for hydrothermal coating. Disks were cut with 10 mm diameter and 2 mm thickness from the ingot of AZ91-3Ca alloy. Sample surfaces were prepared using 800, 1,000, 1,200, and 1,500 grit size SiC paper and then ultrasonically cleaned in ethanol for 10 min prior to coating. Two variants CP4100 (pH 4, 100°C and 3 h) and CP7100 (pH 7, 100°C and 3 h) were produced for this study because they have the optimum corrosion rate and higher shear strength as reported in our previous work (Ali et al., 2019) which fulfills the shear strength criteria of bioactive coatings as per ISO 13779-4. Thus, this work mainly focuses on the prolonged degradation behavior of coated and uncoated AZ91-3Ca magnesium alloy and its response to pre-osteoblast MC3T3-E1 cells. Furthermore, the mechanical strength of coated samples as a function of degradation time has also been investigated.

Characterization

The surface morphology and elemental composition of the samples were analyzed using variable pressure Scanning Electron Microscope (SEM) Vega LMU from TESCAN Brno, Czech Republic equipped with Inca X-Act EDS detector from Oxford Instruments, Oxford United Kingdom.

The phase analysis of the deposited coatings was done using a PANalytical X'pert powder X-ray diffractometer from Philips, Netherlands over the range of 20°–80° with the step size of 0.02° and count time of 1 s per step.

Immersion Test

The degradation behavior of coated and uncoated AZ91-3Ca alloy was investigated using *in vitro* immersion test in SBF according to ASTM-G31-72 (American Society for Testing Materials, 2004). The SBF was prepared by adding certain reagents in the order given in **Table 1** (Ali et al., 2019).

All the samples were immersed in SBF (pH 7.35) a day after preparation to ensure its stability. Before immersion, the samples were dried in an oven at 80°C for 1 h and weighed using microbalance. As the magnesium corrodes in a physiological environment, complex degradation products including calcium and phosphorus ions formed on sample surfaces. Thus, a high solution volume to sample surface area ratio (30 ml cm^{-2}) was used in this study. Such a high ratio was used to ensure that during the test, calcium and phosphorus ions concentration does not change significantly and it mimics the *in vivo* environment for a given time. The prepared samples with an average surface area of 0.7 cm^2 each, were immersed in a 20 ml of SBF solution to fulfil 30 ml cm^{-2} surface area to volume ratio condition. The SBF was never refreshed throughout the entire period of experiment. For these experiments, a syringe method previously reported by Rahim et al. (2017) was used. This technique was adopted due to its simplicity, cost-effectiveness, less workspace requirement, multiple samples test at the same time (**Figure 1**), and easiness in the collection of quality data from single experiment.

A 20 ml syringe with a 21G needle was used as a test container. To insert the samples the plungers were pulled out and samples were loaded, and then the plungers were inserted back. 20 ml of SBF solution was sucked into the syringes, followed by stationary incubation at 37°C in a drying oven for 1 day, 3, 7, 14, and 28 days. The test was performed in a triplicate manner with a rectangular bar-shaped sample having an average dimension of 10 mm × 2 mm × 2 mm i.e. length, width, and height, respectively. For each variant and time interval, a separate syringe was used to avoid any interruption in the experiment. All the syringes were hanged in a drying oven in such a way that the syringe tips were pointing downwards (**Figure 1**). Control syringes filled with 20 ml of SBF carrying no samples were also used to ensure that no solution expels from the syringe without any chemical reaction. It was assumed that no solution was lost to evaporation as the experiment was executed under a closed environmental condition. Each bubble of hydrogen generated due to

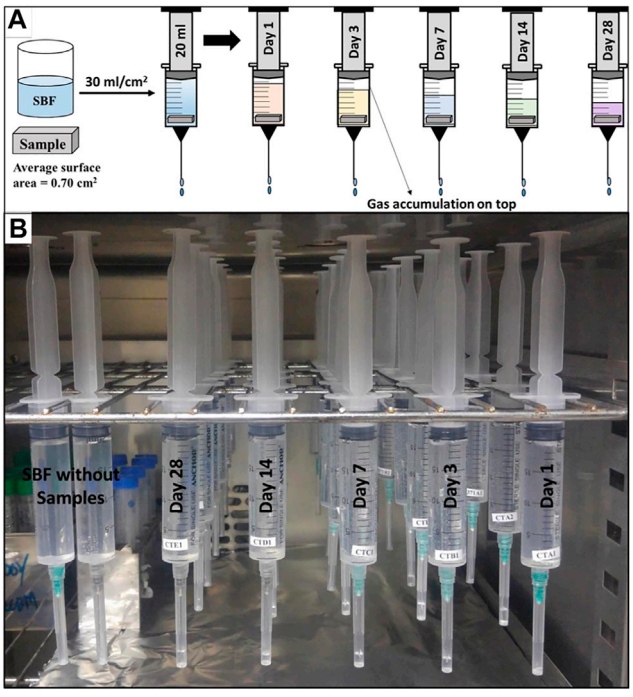

FIGURE 1 | (A) Drawing of the immersion test assembly **(B)** Immersion test setup in incubator.

magnesium corrosion expel an equal amount of solution from the syringe (see **Eq. 1**). Thus, after each time interval, the volume of SBF solution left in the syringe was measured and difference in initial and final volume was recorded as hydrogen evolution (HE). This was later used to calculate the hydrogen gas evolution rate (HER). The pH of corrosion media after each time interval was measured using standard portable pH meter MW 101 from Milwaukee, United States. The pH meter was calibrated at each time before use as per the manufacturer's protocol.

$$Mg + 2H_2O \rightarrow Mg(OH)_2 + \uparrow H_2. \quad (1)$$

The samples were removed from syringes, gently rinse with distilled water, and dried in an oven at 80°C for 2 h. The dried samples were weighed again, visually inspected, and photographed. The difference in the final weight of samples (W_i) after each immersion time interval and initial weight (W_o) was calculated and plotted as experimental weight loss.

The corrosion rate (CR) was calculated from the total volume of hydrogen evolution (CR_H) and weight loss (CR_W) using **Eq. 2** and **Eq. 3** respectively (Johnston et al., 2018).

$$CR_H = 2.088\frac{V_H}{At} \quad (2)$$

$$CR_w = 2.1\frac{\Delta m}{At}, \quad (3)$$

To get the CORROSION RATE (CR) in a unit of mm/year, weight change (Δm) in milligram, total hydrogen evolution volume (V_H) in milliliter, surface area (A) in centimeter, and immersion time (t) in days were measured.

Mechanical Testing of Coated and Uncoated AZ91-3Ca Alloy

To determine the effect of degradation time on strength of coated and uncoated AZ91-3Ca alloys, uniaxial compression tests have been conducted after each time interval of immersion. Samples recovered from immersion tests were cut with a dimension of 5 mm × 2 mm × 2 mm i.e. length, width and thickness, respectively using Micracut 151 from Kemet International Ltd., United Kingdom. After cutting, the samples were thoroughly rinsed with distilled water followed by oven drying. Compression tests were conducted at a constant strain rate of $10^{-3}\,s^{-1}$ until failure using an electrodynamic fatigue testing system equipped with a 1.5 kN high-resolution load cell from Walter + Bai AG, Switzerland. The compression strength of each sample was determined and the results after each time interval of immersion up to 14 days were compared.

Cell Culture, Proliferation, and Cell Attachment Assays

MC3T3-E1 cells were cultured in Alpha Minimum Essential Medium (α-MEM) supplemented with 10% FBS and 1% Penicillin/Streptomycin. Cytotoxicity of coated magnesium alloy; CP4100 and CP7100, and uncoated AZ91-3Ca alloy was assessed using the Alamar Blue (AB) assay for 3 days. Before cell culture, all the discs were autoclaved. The 1×10^4 cells were seeded at the tissue culture plate (TCP) and coated and uncoated AZ91-3Ca alloy were immersed using transwell inserts for avoiding direct contact of sample with cells. All the samples were used in triplicate. MC3T3-E1 cells seeded without sample discs were used as a positive control. At day 1 and day 3, AB solution was directly added to the medium resulting in a final concentration of 10% and incubated for 4 h at 37°C. 100 µl of the media was transferred to 96 wells plate and optical density (Tian et al.) of the plate was measured at 550 and 620 nm using microplate reader PR 4100 from Bio-Rad Laboratories, United States.

MC3T3-E1 was used to see the attachment of the cells on the coated and uncoated magnesium AZ91-3Ca alloy. Cells were grown on the coated samples for 3 days. At day 3, 4% paraformaldehyde (PFA) solution was used to fix the cells. Afterward, washing was performed using PBS. Dehydration was carried out using 30, 50, 70, 80, 90 and 100% ethanol concentrations. Scanning Electron Microscopy was performed to check the adherence of cells on the coated and uncoated magnesium alloy discs.

Gene Expression Analysis via qRT-PCR

To evaluate the effect of CaP coated magnesium alloy on bone development at the molecular level, mRNA expression of different osteoblast differentiation and bone formation markers were assessed in the MC3T3-E1 Pre-osteoblast cell line. In brief, RNA was extracted from MC3T3-E1 cells using TRI reagent and cDNA was synthesized from 1 µg RNA by using a cDNA synthesis kit (Invitrogen, United States). Subsequently, qRT-PCR was carried out using a master mix (Maxima Syber Green, Fermentas, United States) and reactions were carried out on PikoReal 96 (Thermo Scientific, United States). Glyceraldehyde 3-phosphate dehydrogenase (GAPDH) was used as internal control and relative expression was analyzed using quantification cycle values. Primer sequences used in this study are given in **Table 2**.

Statistical Analysis

The results are reported as the average values for at least three samples. An unpaired two-tailed t-test was implemented to calculate the statistical significance of the results using a significance level of $p < 0.05$.

RESULTS

Morphological and Phase Analysis

The detailed morphology, crystal structure, and deposition mechanism has been reported in our previous work (Ali et al., 2019). Briefly, the deposited coatings were a mixture of granular material and plate-like structure as evidenced in **Figure 2A** and **Figures 3B,C**. CP7100 coating has a higher amount of granular material in comparison to CP4100 coating. Thick and irregular-shaped plates were deposited on CP4100 samples that densely covered the sample surfaces with no visible cracks. At pH 7, rectangular plates and granular

TABLE 2 | Primers sequences used for qRT-PCR.

Gene	Forward primer (5′-3′)	Reverse primer (5′-3′)
RUNX2	ATTCCTGTAGATCCGAGCACC	GCTCACGTCGCTCATTTTGC
COL1A1	CGTGACCAAAAACCAAAAGTGC	GGGGTGGAGAAAGGAACAGAAA
ALP	ATGGGATGGGTGTCTCCACA	CCACGAAGGGGAACTTGTC
GAPDH	CTGACTTCAACAGCGACACC	AGCCAAATTCGTTGTCATACC

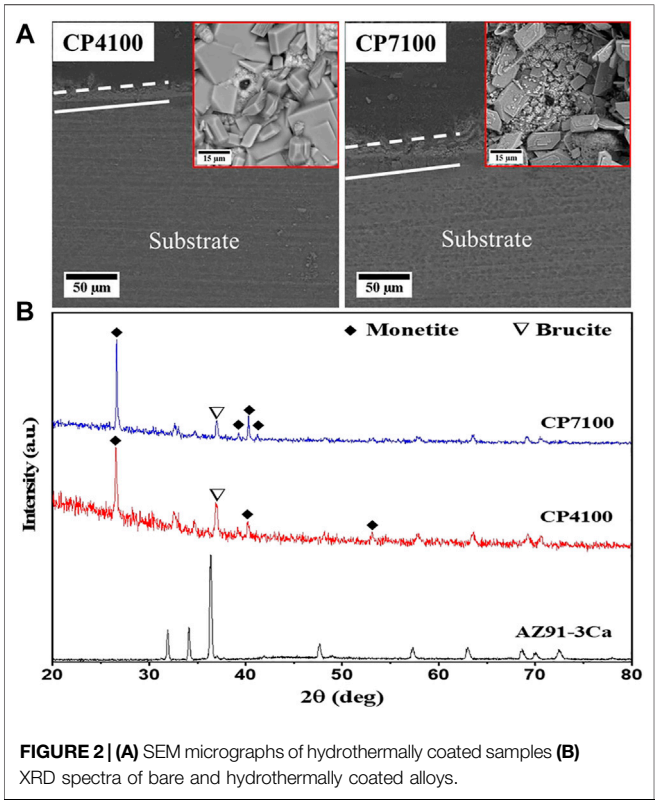

FIGURE 2 | (A) SEM micrographs of hydrothermally coated samples **(B)** XRD spectra of bare and hydrothermally coated alloys.

material densely covered the surface with no visible micro-crack. These plates were uniform in size and non-uniform in distribution.

It is evident from the cross-sectional view (**Figure 2A**) that the deposited coating consists of two layers and coating thickness increases with increasing pH. The average coating thickness of CP4100 coating is 21 μm and CP7100 coating is 29 μm. Both the coating variants have internal and interfacial cracks that increase in numbers with increasing solution pH but no pores were observed in a cross-sectional view of coatings.

The main phases identified in coatings are Monetite ($CaHPO_4$, dicalcium phosphate anhydrous) according to JCPDS 01-0711759, and brucite ($MgO{\cdot}H_2O$, Magnesium Oxide Hydrate) according to JCPDS 00-002-1395. Sharp peaks of Monetite were prominent at both pH values (**Figure 2B**). The full width at half maximum of Monetite

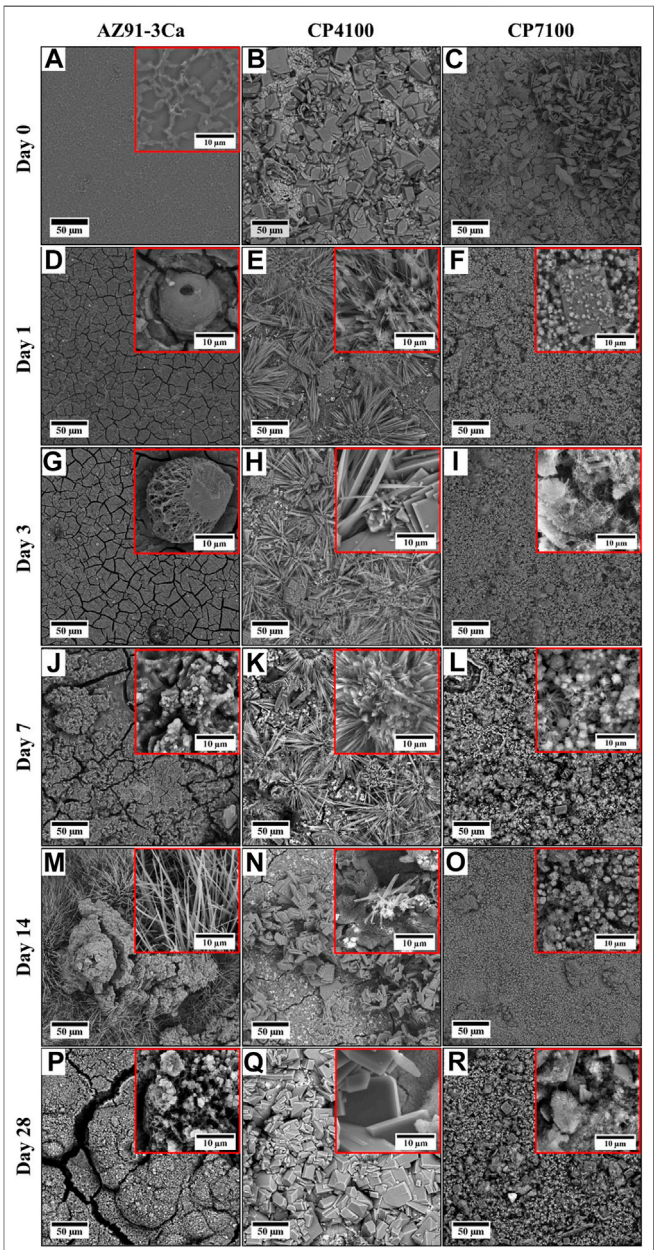

FIGURE 3 | SEM micrographs of coated and uncoated AZ91-3Ca alloy before and after immersion in SBF.

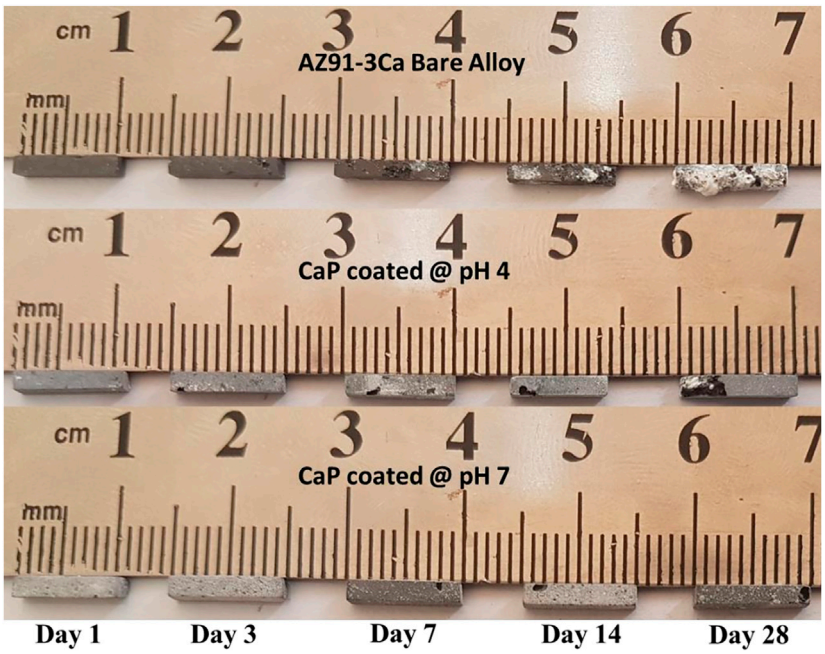

FIGURE 4 | Macrographs of coated and uncoated samples at each prescribed time point of immersion testing in SBF.

(200) peak was found to be 0.10–0.15, suggesting that the crystallinity of Monetite is relatively high.

Qualitative Analysis of Coated and Uncoated AZ91-3Ca After Immersion in SBF

Macrographs of the degraded bar-shaped specimens including CP4100, CP7100 coated AZ91-3Ca, as well as AZ91-3Ca bare alloy control samples after different intervals of immersion time in SBF, are shown in **Figure 4**. The degradation products were continuously deposited on the surface of all the samples. At day 3 of immersion, cracks and pits were witnessed on the edges of CP4100 and bare AZ91-3Ca alloy samples but the CP7100 coating remained intact. After day 7 of immersion, pits were originated on the edges of all the samples. Although the corrosion pits were prominent in all the samples however this localized attack on CP7100 was not as severe. The small crystal features that were started to form on the surface soon after the immersion are now becoming visible to the naked eye. These crystal features grew larger in size and numbers, on the surface of all samples as immersion continued. After 28 days of immersion, the highest amount of these crystal formations was observed on the surface of the bare AZ91-3Ca alloy. Furthermore, the coated samples were able to retain their rectangular shape, but the bare alloy lost its shape and mechanical integrity after 28 days of immersion due to severe localized corrosion. CP7100 coated samples performed well and retained structural integrity in comparison to other tested variants.

SEM micrographs of coated and uncoated AZ91-3Ca alloy samples before and after each interval of immersion are presented in **Figure 3**. It is observed that the surface morphologies of all the samples remarkably altered even after day 1 of immersion in SBF. After 1 day of immersion an oxide layer having cracks formed on the entire surface of the bare AZ91-3Ca alloy sample (**Figure 3D**. A needle-like shaped structure was formed on the CP4100 coatings (**Figure 3E**) while very fine cubical and rods-like structures were formed on the CP7100 coatings (**Figure 3F**). After 3 days of immersion, the passivation layer formed on the surface of the bare alloy becomes thicker with increased crack density on the surface (**Figure 3G**). All the structures formed on CP4100 and CP7100 samples get finer and denser (**Figures 3H,I**). More corrosion product was formed on the bare AZ91-3Ca alloy after 7 days of immersion forming a thick and cracked corrosion layer as shown in (**Figure 3J**). The cracks present on the surface of bare alloy get wider, leaving open spaces for easy solution penetration and making the substrate surface vulnerable to rapid corrosion. No structural changes were observed in CP4100 and CP7100 samples after 7 days of immersion except a whitish granular layer with the growth of crystalline phases as evidenced in **Figures 3K,L**. After 14 days of immersion, the formation of chunky and needle-like microstructures on bare AZ91-3Ca alloy surface was observed (**Figure 3M**). On the other hand, the needle-like structure of the CP4100 sample at day 7 is now completely transformed into an irregular size chip-like structure exposing the passivation layer and underlying cracks of the deposited coating (**Figure 3N**). The fine-grained microstructure formed on the CP7100 sample grown further to form a dense layer of fine globular-shaped structure with no visible cracks on the entire sample surface (**Figure 3O**). After 28 days of immersion needle-like shape structure previously formed on bare AZ91-3Ca alloy surface has been completely transformed into thick islands of the corrosion product having thickest and widest cracks on the entire sample surface (**Figure 3P**). Contrary to this, the surface morphology of CP4100 remains the same after 28 days

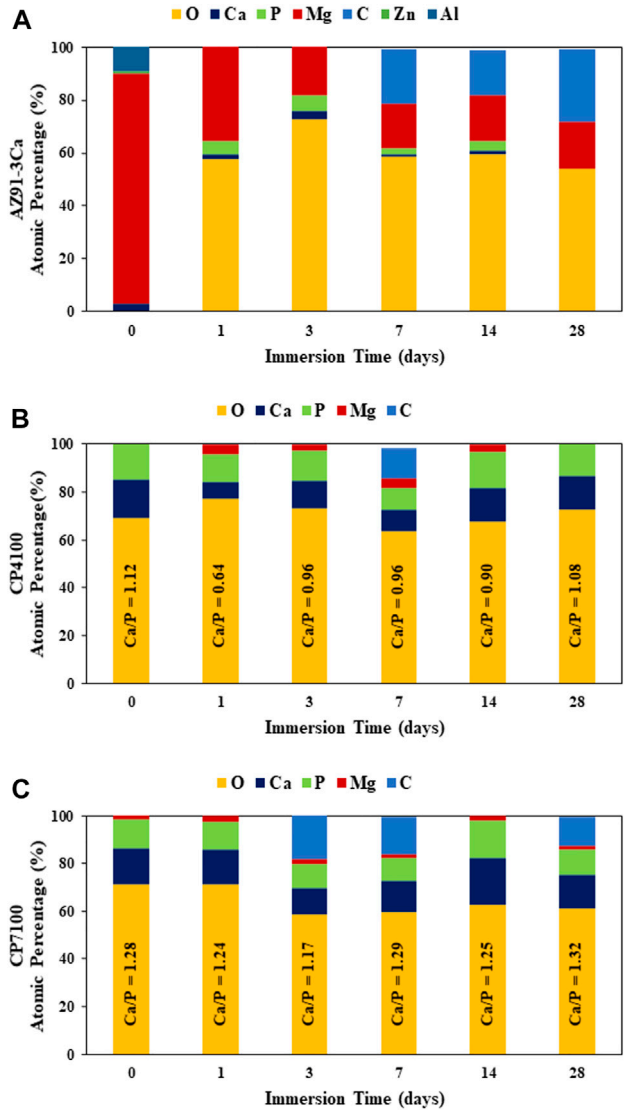

FIGURE 5 | Surface elemental composition (at%) of samples, before and after immersion at prescribed time points in SBF for 28 days, quantified on respective SEM images of **Figure 3** at ×250 magnification using EDS analysis, **(A)** Bare AZ91-3Ca alloy **(B)** CP4100 coated alloy **(C)** CP7100 coated alloy.

of immersion except, the fine chip-like shaped structure grows into a thick rectangular shaped structure that almost covers the entire sample surface (**Figure 3Q**). Similarly, no morphological changes were observed in the CP7100 sample except the growth of the previously deposited granules on the coating surface (**Figure 3R**). Overall, all the samples show deposition of corrosion product and surface defects after immersion in SBF for 28 days but the bare AZ91-3Ca alloy control sample was highly affected while CP7100 shows no remarkable surface defects.

The EDS analysis confirms the presence of Ca, P, Mg, O, and C in all the samples. CP7100 had the highest ratio of Ca to P and the lowest content of Mg among all samples. This depicts higher calcium phosphate deposition indicating better preservation of this coating during the immersion testing. EDX on as-deposited coatings showed the presence of only magnesium/calcium phosphate phases prior to immersion in SBF. However, Post-Immersion EDS analysis indicates the emergence of magnesium and/or calcium carbonate phases along with the calcium phosphate phases as evidenced by the presence of carbon (over 10 atomic %) in all the samples (**Figure 5**). The emergence of the carbonate phases starts at different time intervals in the bare, CP4100, and CP7100 coatings (**Figure 5**).

Quantitative Analysis of Coated and Uncoated AZ91-3Ca After Degradation in SBF

Table 3, presents the results of the corrosion rate calculated from the immersion test data for each sample. **Eq. 2** and **Eq. 3** have been used to convert the hydrogen evolution and weight loss data into corrosion rates. These equations present the corrosion data in a surface area normalized form. Bare magnesium alloy showed the highest and CP7100 showed the lowest average corrosion rate amongst all. Corrosion data calculated from weight loss (CR_w) and hydrogen evolution (CR_H) showed (Zai et al., 2015) a considerable amount of variation between each material group and (ASTM) CR_H was typically smaller than CR_w for all samples and presented as CR_H to CR_w ratio in **Table 3**. These results are in line with previously reported observations in simulated body fluids such as HBSS (Johnston et al., 2015; Johnston et al., 2018). The CR_H to CR_w ratio closer to 1, indicates that hydrogen is produced at a much faster rate than would be expected from the amount of weight loss. It is physically impossible and suggesting that there is an error in the experiment or the collection of hydrogen (Johnston et al., 2018). The observed CR_H to CR_w ratio in this study is far from 1 which indicates the authenticity of the data.

The volume of the observed hydrogen evolution accumulated at top of the syringe, normalized to the surface area of the coated and uncoated magnesium alloys during 28 days of immersion in SBF is presented in **Figure 6A**. On the first day of immersion, a high HER was observed and the highest amount of gas accumulation was detected. On day 3, the rate of gas evolution becomes moderate and then calmed up to day 14. No significant difference in the amount of gas accumulation was detected in all-time points between day 3 and day 14. At day 28 of immersion, once again a little amount of gas accumulation was detected with relatively low HER as compared to the early stage of degradation. A significant difference was noticed in the hydrogen evolution of coated and uncoated magnesium alloy samples at all intervals of immersion testing. To sum it up, bare AZ91-3Ca magnesium alloy showed the highest while CP7100 coated sample showed the lowest hydrogen evolution rate (HER) for 28 days of immersion, respectively.

Figure 6B shows the values of pH of the electrolyte after each immersion interval of coated and uncoated AZ91-3Ca samples. Before immersion test, the pH of SBF was adjusted to 7.4 and it increases at a considerable rate in all the samples with increasing duration of immersion. At day 1, an insignificant difference in pH of SBF was noticed. After 1 day of immersion, the increase in pH

TABLE 3 | Average corrosion rates calculated from immersion test data presented with a ratio of CR_H to CRw for comparison.

Material	Samples	CR_w (mm/year)	CR_H (mm/year)	Ratio CR_H:CR_w
AZ91-3Ca	2	1.73 ± 0.31	0.19 ± 0.04	0.11
CP4100	2	0.92 ± 0.15	0.13 ± 0.03	0.14
CP7100	2	0.72 ± 0.21	0.09 ± 0.01	0.12

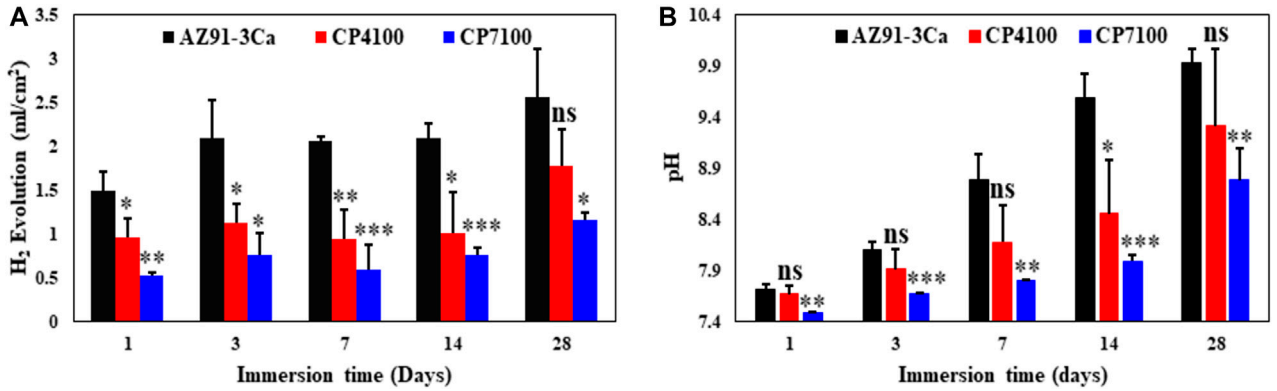

FIGURE 6 | Material degradation at different immersion time **(A)** Hydrogen evolution volume, surface area normalized, produced by coated and uncoated Mg alloy. **(B)** Variation in pH value of the solution of coated and uncoated Mg alloy.

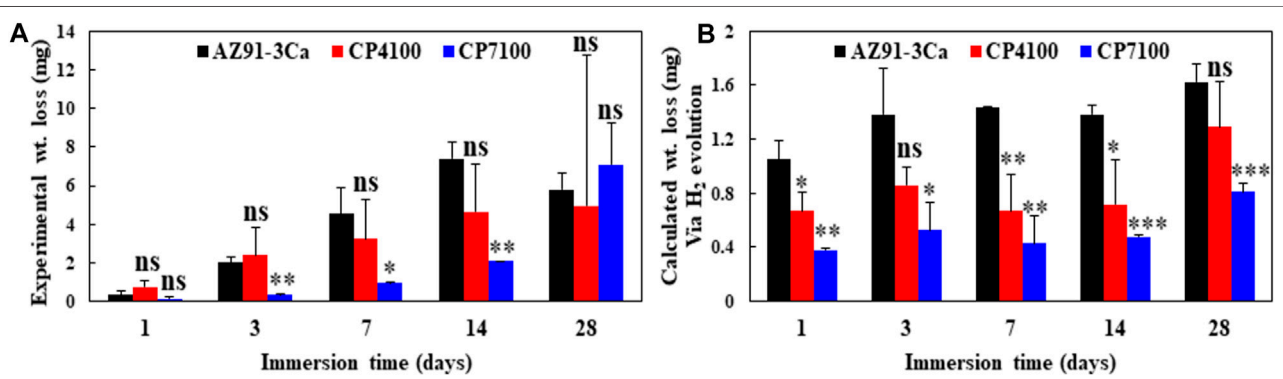

FIGURE 7 | Material degradation at different immersion times **(A)** Experimentally calculated weight loss of coated and uncoated AZ91-3Ca alloy **(B)** Weight loss of coated and uncoated AZ91-3Ca alloy calculated using **Eq. 1** and H_2 evolution data.

of SBF became more significant with each time point. Up to 14 days of immersion, the rate of increase in pH of SBF cultured with bare AZ91-3Ca magnesium alloy was higher which became moderate at day 28. In contrary to this, coated samples show a steady rise of pH level up to day 28 while the overall pH values of coated samples were lower than the bare alloy samples. Evidence from the above results indicated that, after 28 days of immersion, the CP7100 sample shows the least increase in pH among all the samples followed by CP4100 and AZ91-3Ca samples.

The mass changes of coated and uncoated magnesium samples during immersion in SBF for 28 days are summarized in **Figure 7**. It was observed that all the samples exhibited weight loss starting from day 1. After 14 days of immersion, among all the samples, CP7100 coated magnesium alloy showed the least weight loss followed by CP4100 and bare AZ91-3Ca magnesium alloy. Bare magnesium alloy acting as a control sample showed the highest weight loss up to 14 days remaining only 85% of its original weight. The weight of the sample increased to 90% after 28 days of immersion due to the deposition of degradation products on the sample surface as evidenced in **Figure 4**. A similar trend was observed in CP4100 samples with 93% remaining weight after 28 days of immersion in SBF. Experimental as well as theoretical weight loss using stoichiometric calculations has been assessed to differentiate, understand and eliminate the effects/errors, which occur during experimental procedures (**Figures 7A,B**).

Compression Strength of Coated and Uncoated AZ91-3Ca Alloy After Immersion

The compressive strength of coated and uncoated AZ91-3Ca magnesium alloy has been determined after each interval of immersion. The results of compression tests are summarized in **Figure 8**. Before immersion, the compression strength of bare alloy was measured as 383.2 MPa. After day 1 of immersion, the bare alloy possesses the highest (319.52 ± 10.47 MPa) while CP4100 samples have the lowest (231.8 ± 59.69 MPa) compression strength among all. With the increase in the immersion time, the compression strength of all the samples decreases considerably. The compression strength of bare AZ91-3Ca alloy decreases at a rapid rate among all samples due to the high corrosion rate thus after 3 days of immersion no representative sample was left to perform a compression test (**Figure 4**). Consequently, no compression results were obtained for this sample immersed on day 7 and 14. CP7100 sample showed the highest compression strength (259.0 ± 10.65 MPa) after 14 days of immersion in SBF among all the samples indicating the protective nature of the coating. Quantitatively, 9.76 and 12.42% reduction in compressive strengths of CP7100 and CP4100 samples were observed after 14 days of immersion as compared to 1 day of immersion.

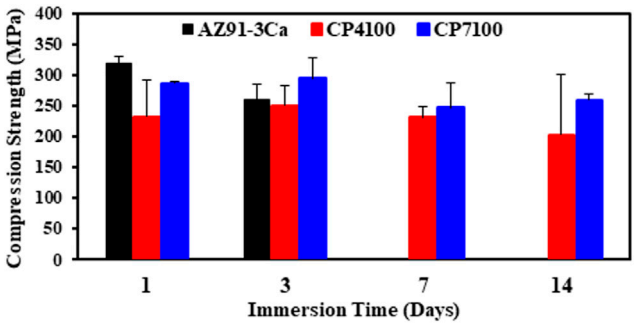

FIGURE 8 | Compression strength of coated and uncoated Mg alloy during immersion testing in SBF.

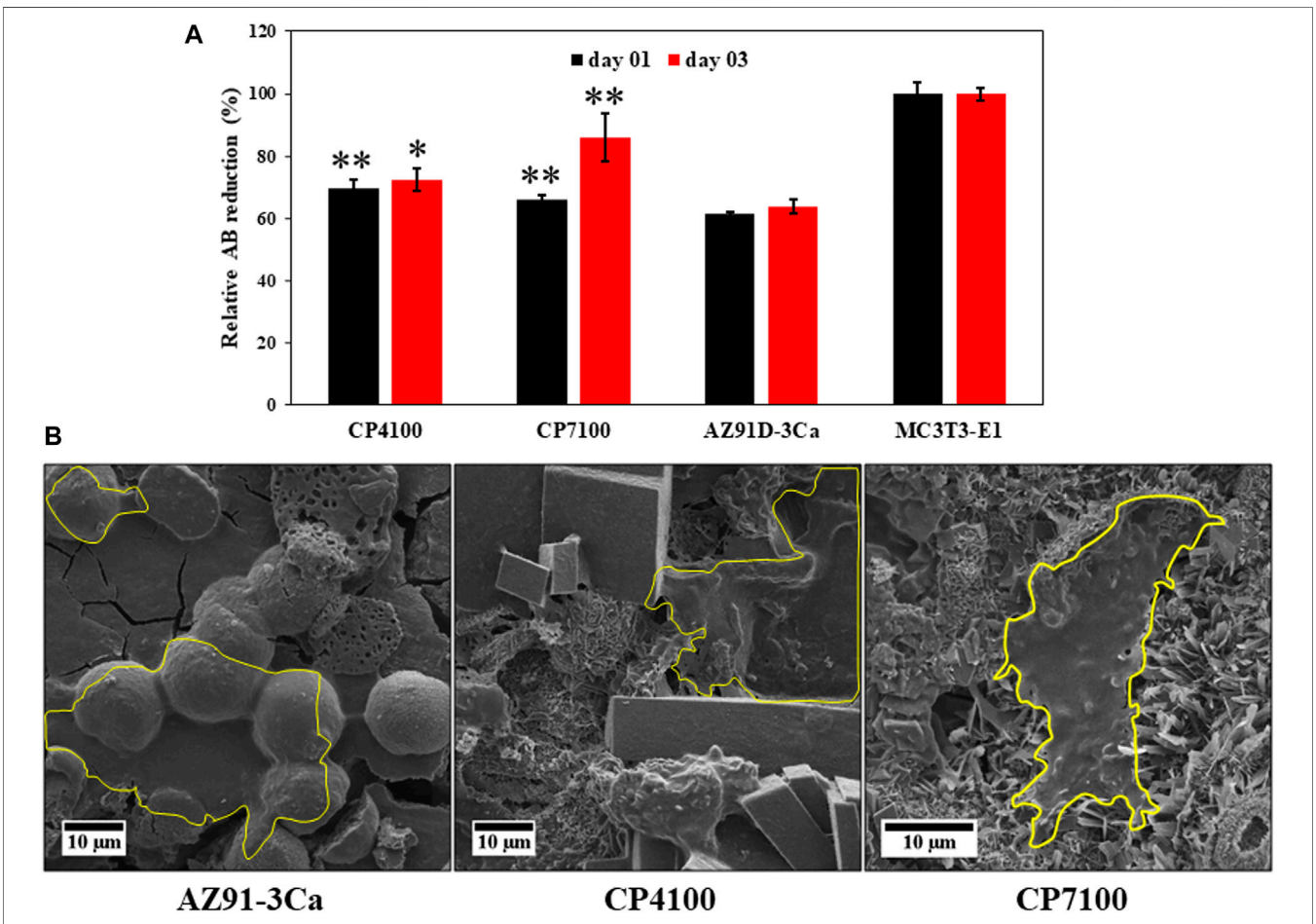

FIGURE 9 | (A) metabolic activity of MC3T3-E1 pre-osteoblast cell measured by Alamar blue assay at day 1 and 3 for coated and uncoated Mg alloy and MC3T3-E1 cells and **(B)** SEM micrograph of MC3T3-E1 cell attachment on coated and uncoated sample surface fixed using 4% paraformaldehyde after 3 days of culturing. Cell attachment region is highlighted in yellow boundary.

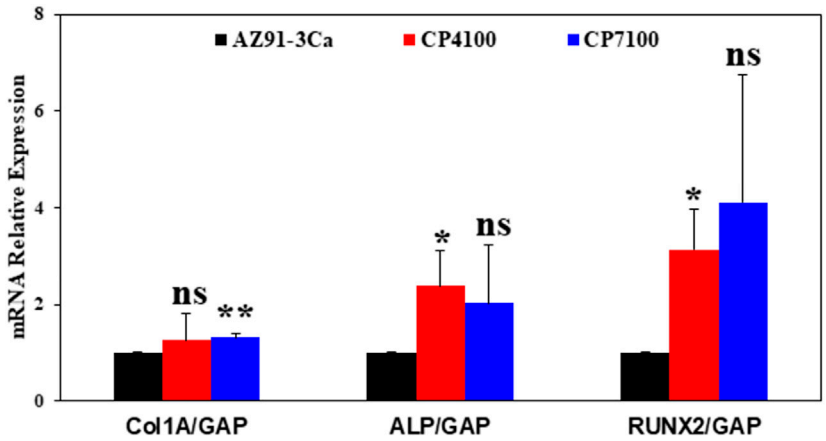

FIGURE 10 | Gene expression analysis of osteoblast differentiation and bone formation markers: Relative mRNA expression levels of Col1A, ALP and RUNX2. GAPDH was used as loading control. Values were expressed as mean ± SD (n = 4, each). *$p \leq 0.05$ vs. control group.

Cell Proliferation and Adhesion Assays

The relative differences in metabolic activity of MC3T3-E1 cells cultured in the presence of CaP coated AZ91-3Ca alloy; CP4100 and CP7100 and uncoated AZ91-3Ca alloy were determined using Alamar blue (AB) assay (**Figure 9A**). It was revealed that the CaP coated magnesium alloy provides an enabling environment for the cells as made obvious by the reduction of AB on day 3. An increase in cell proliferation in the case of CaP coated magnesium alloy was noticed as compared to uncoated AZ391-3Ca alloy. The reduction of AB by the MC3T3-E1 cells grown in the presence of CaP coated magnesium alloy was comparable to the control cells, which were grown on the tissue culture plate.

To study the attachment of the pre-osteoblasts MC3T3-E1 cells on CaP coated magnesium alloy, the cells were fixed with 4% PFA after day 3. The results disclosed that the surfaces of the coated magnesium alloy were highly impregnated with cells covering a large space forming confluent sheets over the surfaces of CaP coating as displayed in **Figure 9B**. The attachment of cells on the magnesium alloy discs can be linked to moderate confluency of the cells. This data indicates that CaP coatings on AZ391D-3Ca provided a suitable environment to the cells to attach, grow and adhere to these friendly surfaces using filopodia. These are cytoplasmic projections that help in substrate-cell interaction (Stachewicz et al., 2015).

Gene Expression Analysis of Bone Differentiation Markers by qRT-PCR

CaP coated magnesium alloy enhances the expression of osteoblast differentiation marker. To access the effect of CaP coated magnesium alloy on osteoblast biology, the expression level of COL1A, ALP and RUNX2 were determined in MC3T3-E1 cells. It was observed that the expression of COL1A and ALP markedly up-regulated in CaP coated AZ91-3Ca alloy as compared to bare AZ91-3Ca alloy. However, highest significant increase was noted in RUNX2 mRNA expression (CP7100, 4.1 ± 2.6 fold, $p < 0.05$; CP4100, 3.1 ± 0.8 fold; AZ91-3Ca, 1 ± 0 fold) as shown in **Figure 10**.

DISCUSSION

Generally, it takes 4–12 weeks to repair a bone depending on the individual's ability to heal, implant type, and anatomical location of the bone. Therefore, magnesium-based implants must retain their mechanical strength and integrity for a minimum of 12 weeks for the fracture to stabilize. The main role of CaP coatings is to reduce the degradation rate, minimize the initial burst of hydrogen evolution, and improved mechanical strength of an implant. In consequence, these factors will accelerate the bone healing process. The results of the previous findings by Ali et al. (2019) showed that high strength CaP coatings produced via a single-step hydrothermal method significantly improved the corrosion resistance with no sign of cytotoxicity when cultured with NIH3T3 fibroblast cells. However, in this study, the prolonged degradation behavior and its effect on the mechanical properties of CaP coated and uncoated AZ91-3Ca magnesium alloy was studied. Moreover, osteogenic differentiation and osteogenic gene expression analysis were also examined.

Formation of Degradation Product and Structural Changes

Figure 3 and **Figure 4** display the macro and micro images of samples respectively after different intervals of immersion in SBF. It is evident from the visual observation that uncoated samples (Bare AZ91-3Ca alloy control) have been severely attacked and damaged after soaking in SBF for 28 days (see **Figure 4**). Among all the coated samples shown in **Figure 4**, CP7100 coatings showed the least macroscopic damage due to least corrosion and degradation during entire period of immersion i.e. 28 days.

Microscopic evaluation of degradation behavior of all the samples over the entire period of 28 days is shown in **Figure 3**. During immersion in SBF, the coated sample morphology significantly changes in comparison to as coated state (**Figures 3A–C**). As soon as the bare AZ91-3Ca alloy sample was immersed in SBF, their surfaces start reacting with the solution according to **Eq. 1** which steeply increase the localized pH at the sample surface irrespective of the pH of the solution (Ali et al., 2019). This leads to the precipitation of $Mg(OH)_2$ and calcium/magnesium phosphate phases as confirmed by the EDS spectra of the sample after day 1 (**Figure 5A**) which covers the entire sample surface (**Figure 3D**). A similar trend was observed in coated samples where after day 1 of immersion Mg, Ca, and P content increases (**Figures 5B,C**). This indicates the deposition of magnesium phosphate phase along with the deposition of hydroxyapatite from physiological solution. Moreover, the transformation of already deposited monetite phase to hydroxyapatite phase takes place which results in refinement of coating microstructure (**Figures 3E,F**). It is also worth noticing that because of solution penetration, the calcium phosphate layer on CP4100 coating became loose and fallout into the solution to result in the lower content of Ca and P as affirmed from EDS analysis (**Figure 5B**). After day 3, more HA was formed on bare alloy (control sample) and CP4100 sample surfaces, which was observed as white dots in **Figure 3G** and dense cactus-like shape structure in **Figure 3H** respectively as substantiated by EDS analysis (**Figures 5A,B**). It is presumed that, this small amount of hydroxyapatite (HA) precipitated out from SBF through the biomimetic process and that its adhesion strength would be low as reported in the literature (Guan et al., 2012). It appears that Mg content in bare alloy after day 3 decreases which is not true. The reason to this is, an increase in the thickness of the surface corrosion layer, which limits the Mg peak in EDS analysis originating from the substrate. CP7100 sample shows an increase in Mg content and presence of C content (**Figure 5C**) indicating the formation of the carbonate phase. At day 7 of immersion, all the samples showed a significant amount of carbon in EDS analysis (**Figure 5**). It is speculated that some carbonate phases ($CaCO_3$/$MgCO_3$) precipitated on all the sample surfaces (**Figures 3J–L**), which correlate with previously reported literature (Zou et al., 2016; Tian et al., 2019; Öcal et al., 2020; Zeller-Plumhoff et al., 2021) that corrosion products formed on surfaces include $CaCO_3$ and $MgCO_3$ phases after immersion in physiological solutions. The carbonate phase improves the passivation of the surface and impedes further corrosion as demonstrated by hydrogen evolution (**Figure 6A**) and weight loss (**Figure 7**), while $Mg(OH)_2$ as a corrosion product hardly provide any protection from degradation (Zou et al., 2016). It is given in the literature (Tian et al., 2019) that $CaCO_3$ coating improves the cell adhesion on the sample surface as compared to non-coated magnesium alloy. After day 14 of immersion Mg and P content increases in the bare alloy sample (**Figure 5A**). This implies the formation of some magnesium phosphate phase as supported by SEM micrograph (**Figure 3M**) has a needle-like shaped structure. In case of both coating variants, all the carbonate disappeared and the Ca and P amount increases (**Figures 5B,C**) after day 14 indicates the formation of calcium phosphate phase as reported in the literature (Zeller-Plumhoff et al., 2021) that increase in Ca and P amount refer to the formation of hydroxyapatite. It is presumed that previously deposited carbonate (At day 7) reacted with the phosphate present in physiological solution to form the calcium phosphate phases e.g. hydroxyapatite. This newly formed hydroxyapatite could be Mg-doped or some other magnesium phosphate/oxide phase formed because the surface EDS analysis (**Figures 5B,C**) showed a minor increase in the amount of Mg in coated samples. After day 28 of immersion, the only degradation product present on the bare alloy surface was magnesium carbonate as established by EDS analysis (**Figure 5A**) and evidenced in **Figure 4** as white precipitates. No magnesium was observed in CP4100 samples, which attributed to complete surface coverage with calcium phosphate phase as evidenced in **Figure 3Q**. The magnesium peak instigating from the magnesium phosphate/oxide phase vanished because the precipitated phase could be inadequately clung to the surface and fallout into the solution or react with the solution to form some soluble salt. The decrease in Ca content and increase in P amount (**Figure 5B**) can be attributed to the formation of some other P rich calcium phosphate phase and/or calcium deficient hydroxyapatite. In case of CP7100 samples, some carbonate phase deposition was observed along with the decrease in Ca, Mg, and P content (**Figure 5C**). This lead to a presumption that a sort of chemical equilibrium was established on day 7 and a cyclic process started in which the carbonate phase transformed into the calcium phosphate phase over the period of 7 days and vice versa. Overall, $Mg(OH)_2$, $CaCO_3$, and HA phases precipitated on the sample surfaces as corrosion products during immersion of HA-coated magnesium samples as reported in literature (Guan et al., 2012) and in agreement with the results of this study. The precipitation of these corrosion products restricts further penetration of solution to the substrate resulting in improved corrosion resistance of CP7100 coatings by filling their internal cracks, defects, and covering the surfaces. In contrast, precipitation products on bare alloy and CP4100 coatings were loosely bounded and could not provide sufficient barrier to inhibit corrosion.

Effect of Coating on Hydrogen Evolution Rate

Hydrogen gas is a degradation by-product of magnesium/magnesium-based alloys that are formed because of an electrochemical reaction (**Eq. 1**). This amount of hydrogen gas produced (**Figure 6A**) in the immersion test may also be utilized for comparing the degradation rate. All the samples showed different hydrogen evolution rates. In bare AZ91-3Ca alloy, an initial burst of hydrogen production (**Figure 6A**) was observed up to 3 days of immersion beyond which the rate decline. Although bare AZ91-3Ca alloy showed a gradual increase in weight loss measurements (**Figure 7**), three different stages were found in HER as directed by **Figure 6**. At the early stage, hydrogen evolution increased gradually but HER decreased after the third day of immersion in SBF. Higher HER at the early phase

of immersion was because of the ease of access of water molecules to the magnesium surface. In the second stage, as immersion time increases, hydrogen production almost stopped after day 3 to day 14. This happens due to the decrease in the degradation rate as the corrosion layer became denser and hinders further penetration of water molecules to sample surfaces. These results are in line with previous findings (Öcal et al., 2020), where decrease in HER, was attributed to the formation of carbonate phase to limits the solution penetration and inhibition of further corrosion.

In the final phase of the immersion test, day 14 to day 28, again a little increase in HER was witnessed and corrosion rate was further increased (**Figure 6A**) which is also supported by weight loss data (**Figure 7**). Likewise, in the study of Ascencio et al. (2015), an increase in the hydrogen gas formation was correlated with increased corrosion rate which induced larger pit formation. Moreover, Song (2005) observed a higher amount of gas formation and increased corrosion rate due to the breaking of protective $Mg(OH)_2$ film by pit formation.

Similar hydrogen evolution regimes were noticed in coated AZ91-3Ca alloy like bare AZ91-3Ca alloy with a relatively lower amount of hydrogen evolution. This shows the protective nature of coatings by providing a more complex path for water molecules penetration to the magnesium substrate surface resulting in a lower dissolution rate. It is concluded, CP7100 had the lowest corrosion rate and HER among all the samples. This was attributed to the dense and thicker coating creating a more complex path for the water molecules to reach the magnesium alloy interface.

Weight Loss Measurements

Figure 4 illustrated that each sample had a different response to SBF due to differences in their degradation rate and localized corrosion. **Figure 7A** shows the average weight loss of each sample at a prescribed time point during 28 days of immersion in SBF. Both, bare alloy and CP4100 exhibited relatively same corrosion trend up to day 3 and after that CP4100 weight loss rate somewhat decreases relative to bare alloy. The lower coating thickness and open coating pores could be responsible for the initial higher degradation rate and later these coating defects filled up by corrosion products leaving no open spaces for solution penetration to the substrate surface resulted in a decreased corrosion rate. A gradual increase in weight loss was observed in all the samples, however, the highest weight loss was observed in bare AZ91-3Ca alloy. Interestingly at day 28, the CP7100 sample, which was showing the lowest weight loss, suddenly showed the highest weight loss contrary to bare alloy and CP4100 (**Figure 7A**). In reality, the actual weight loss trend is the same and the display of this opposite trend is due to the deposition of a large amount of corrosion product on bare alloy and CP4100 sample surfaces (**Figure 4**). This added more weight to the final weight of samples (W_i), reflected as an opposite trend, and gives the lower weight loss readings relative to CP7100. **Figure 7B** displays the calculated (actual) weight loss from a balanced electrochemical reaction (**Eq. 1**) using hydrogen evolution data. Here it is worthy to note that the trend of weight loss presented in **Figures 7A,B** remains the same only the values of weight change decreases. This difference in experimental (**Figure 7A**) and calculated (actual) (**Figure 7B**) weight loss values is due to the undermining of secondary phases from bare alloy and fall out of loose coating particles in case of coated samples. In each syringe, these particles were collected as sediment at the end of the experiment.

Effect of Coating on Mechanical Integrity of Magnesium-Based Implants

Orthopaedic implants like intra-articular screws, when in service, normally undergo compressive and tensile stresses that could lead to unwanted mechanical failure. The mechanical properties of magnesium-based implants could badly be affected by localized corrosion i.e. pitting when coupled with these stresses (Tian et al., 2019). Thus, corrosion resistance of the biodegradable implants should be sufficiently high to reduce the initial degradation rate so that the implant could uphold its mechanical integrity during the bone healing period.

In this work, coated magnesium alloy showed improvement in strength as compared to bare AZ91-3Ca magnesium alloy after immersion in SBF for 14 days (**Figure 8**). It is because calcium phosphate coating boosts the resistance to localized corrosion and hinders the stress-assisted corrosion processes i.e. stress corrosion cracking. CP7100 coated magnesium alloy exhibited the highest average compressive strength (259 ± 10.65 MPa) among all samples. This could be because CP7100 coated magnesium alloy exhibited the lowest degradation and hydrogen evolution rate with intact coatings after 28 days of immersion in SBF. Collectively, CP7100 coated magnesium alloy could support fractured bones and retain structural stability for a longer period than uncoated magnesium alloys, thus providing better mechanical and degradation properties for bone fixation devices.

Effect of CaP Coatings on Cell Viability, Proliferation, Adhesion, and Bone Differentiation

The surface of the materials directly interacts with the cells (Chen, 2016). In our study, we could show that mouse pre-osteoblast cells showed better biocompatibility, viability, and attachment to the coated magnesium alloy as compared to bare AZ91-3Ca magnesium alloy. These data support that CaP coatings on AZ91-3Ca magnesium alloy provide an amicable environment to the cells, which may indicate that these coatings have reduced the degradation rate, hydrogen evolution and low alkaline poisoning effect as evidenced in **Figure 6** and **Figure 7** from the surface thus showed improvement in biological processes when compared it to bare alloy.

Furthermore, expression analysis of bone differentiation markers (*ALP, RUNX2,* and *COL1A*) in these cells after exposing them to coated and bare magnesium alloy was also performed. It was observed that a significant increase in the expression of *RUNX2* at the RNA level in the pre-osteoblast cells which were exposed to coated magnesium alloy. This is in line with the previous studies describing that *RUNX2* is the first transcription factor required for the determination of the osteoblast lineage (Komori, 2009). However, change was also

noticed in the expression of *ALP* expression, which is a downstream target of the *RUNX2* transcription factor (Kirkham and Cartmell, 2007). These data indicate that pre-osteoblast cells started to differentiate to become osteoblasts after proliferating well in the cordial environment provided by coated magnesium alloys. However, an increase in the expression of the *COL1A* gene in the cells exposed to coated magnesium alloy was not noticed, which might be because the cells were not exposed long enough to see the rising level of collagen 1 A.

Altogether, this data indicates that CaP coatings on AZ91-3Ca magnesium alloy provide a very friendly environment for the cell to proliferate and can initiate osteogenic differentiation, which may be used for orthopaedic implants applications in the future.

CONCLUSION

In conclusion, the present study demonstrated that the CaP coatings deposited by the single-step hydrothermal method reduced the degradation rate by 60% and HER by 65% as compared to bare AZ91-3Ca alloy. This slow degradation is responsible for retaining better mechanical properties of coated specimens after immersion as compared to uncoated specimens. The CP7100 coated samples retain 90% of its compressive strength (259.0 ± 10.65 MPa), which still meets the requirements of load-bearing implants. Furthermore, MC3T3-E1 pre-osteoblast cells culturing with coated samples and live/dead assay tests show no significant difference in cell proliferation on coating and positive control. In the cell attachment study, cells showed better biocompatibility, viability, and attachment to the coated magnesium alloy as compared to bare AZ91-3Ca magnesium alloy, which is an indication of improved osteointegration. Moreover, the expression of osteoblastic markers is higher in MC3T3-E1 cells grown on coated substrates than on bare substrates. These results suggest that osteointegration and osteogenesis of magnesium implants in bone tissue should be improved if they are coated with calcium phosphate. Single-step hydrothermal is particularly useful in this regard, as it can generate coating with good substrate adhesion and crystallinity. Such coatings could positively tune the degradation, hydrogen evolution rates and retain the required mechanical properties for the desired timeframe which may end up in stable hard tissue healing.

DATA AVAILABILITY STATEMENT

The raw data supporting the conclusion of this article will be made available by the authors, without undue reservation.

AUTHOR CONTRIBUTIONS

FIq: Conceptualized, designed, supervised and provide technical guidance for all aspects of the project and acquire funding. AA: Conceptualization, Designed, Planned, performed the experiments, analysis, interpretation and acquisition of data. FIk, HF: Performed the cell culturing experiments and analyzed the data, AM: Performed the RT-PCR experiments and analyzed the data. AA, FIk, HF, AM, MK: drafting the manuscript. AA and MK: revising and editing the first draft. FIq, AC, SS and IR: revising the manuscript critically for important intellectual content. All authors contributed to the article and approved the submitted version.

ACKNOWLEDGMENTS

The authors appreciate the financial support of the Higher Education Commission, Pakistan through a financial grant under the National Research Program for Universities No: 20-4388/R&D/HEC/14/684. The authors Thank Professor Mathias Göken from the Institute of General Materials Properties, Friedrich Alexander University of Erlangen Nuremberg, Germany for generously providing AZ91-3Ca alloys.

REFERENCES

Ali, A., Iqbal, F., Ahmad, A., Ikram, F., Nawaz, A., Chaudhry, A. A., et al. (2019). Hydrothermal Deposition of High Strength Calcium Phosphate Coatings on Magnesium Alloy for Biomedical Applications. *Surf. Coat. Techn.* 357, 716–727. doi:10.1016/j.surfcoat.2018.09.016

American Society for Testing Materials (2004). *ASTM G31-72: Standard Practice for Laboratory Immersion Corrosion Testing of Metals*. Philadelphia: American Society for Testing Materials.

Ascencio, M., Pekguleryuz, M., and Omanovic, S. (2015). An Investigation of the Corrosion Mechanisms of We43 Mg Alloy in a Modified Simulated Body Fluid Solution: The Effect of Electrolyte Renewal. *Corrosion Sci.* 91, 297–310. doi:10.1016/j.corsci.2014.11.034

Asl, S. K. F., Nemeth, S., and Tan, M. J. (2014). Hydrothermally Deposited Protective and Bioactive Coating for Magnesium Alloys for Implant Application. *Surf. Coat. Techn.* 258, 931–937. doi:10.1016/j.surfcoat.2014.07.055

Asl, S. K. F., Nemeth, S., and Tan, M. J. (2015a). Improved Corrosion Protection of Magnesium by Hydrothermally Deposited Biodegradable Calcium Phosphate Coating. *Mater. Chem. Phys.* 161, 185–193. doi:10.1016/j.matchemphys.2015.05.035

Asl, S. K. F., Nemeth, S., and Tan, M. J. (2015b). Mechanism of Calcium Phosphate Deposition in a Hydrothermal Coating Process. *Surf. Coat. Techn.* 270, 197–205. doi:10.1016/j.surfcoat.2015.03.003

Biggs, M., Richards, R., Gadegaard, N., Wilkinson, C., and Dalby, M. (2007). The Effects of Nanoscale Pits on Primary Human Osteoblast Adhesion Formation and Cellular Spreading. *J. Mater. Sci. Mater. Med.* 18, 399–404. doi:10.1007/s10856-006-0705-6

Brar, H. S., Platt, M. O., Sarntinoranont, M., Martin, P. I., and Manuel, M. V. (2009). Magnesium as a Biodegradable and Bioabsorbable Material for Medical Implants. *JOM* 61, 31–34. doi:10.1007/s11837-009-0129-0

Chen, J. (2016). "Thin Film Coatings and the Biological Interface," in *Thin Film Coatings for Biomaterials and Biomedical Applications* (Cambridge: Elsevier), 143–164. doi:10.1016/b978-1-78242-453-6.00007-9

D'antonio, J. A., Capello, W. N., Manley, M. T., Geesink, R. G., and Jaffe, W. L. (2004). "Hydroxyapatite Femoral Stems for Total Hip Arthroplasty: 10–14 Year Follow-Up," in *Fifteen Years of Clinical Experience with Hydroxyapatite Coatings in Joint Arthroplasty* (Paris: Springer), 235–241.

Gao, C., Peng, S., Feng, P., and Shuai, C. (2017). Bone Biomaterials and Interactions with Stem Cells. *Bone Res.* 5, 17059. doi:10.1038/boneres.2017.59

Gray-Munro, J., and Strong, M. (2009). The Mechanism of Deposition of Calcium Phosphate Coatings from Solution onto Magnesium Alloy Az31. *J. Biomed. Mater. Res. A: Official J. Soc. Biomater.* 90, 339–350. doi:10.1002/jbm.a.32107

Guan, R. G., Johnson, I., Cui, T., Zhao, T., Zhao, Z. Y., Li, X., et al. (2012). Electrodeposition of Hydroxyapatite Coating on Mg-4.0 Zn-1.0 Ca-0.6 Zr Alloy and *In Vitro* Evaluation of Degradation, Hemolysis, and Cytotoxicity. *J. Biomed. Mater. Res. A* 100, 999–1015. doi:10.1002/jbm.a.34042

Haghshenas, M. (2017). Mechanical Characteristics of Biodegradable Magnesium Matrix Composites: A Review. *J. Magnesium Alloys* 5, 189–201. doi:10.1016/j.jma.2017.05.001

Hiromoto, S., and Tomozawa, M. (2010). Corrosion Behavior of Magnesium with Hydroxyapatite Coatings Formed by Hydrothermal Treatment. *Mater. Trans.* 51, 2080–2087. doi:10.2320/matertrans.m2010192

Hiromoto, S., and Yamamoto, A. (2009). High Corrosion Resistance of Magnesium Coated with Hydroxyapatite Directly Synthesized in an Aqueous Solution. *Electrochim. Acta* 54, 7085–7093. doi:10.1016/j.electacta.2009.07.033

Hornberger, H., Virtanen, S., and Boccaccini, A. (2012). Biomedical Coatings on Magnesium Alloys–A Review. *Acta Biomater.* 8, 2442–2455. doi:10.1016/j.actbio.2012.04.012

Horynová, M., Remešová, M., Klakurková, L., Dvořák, K., Ročňáková, I., Yan, S., et al. (2019). Design of Tailored Biodegradable Implants: The Effect of Voltage on Electrodeposited Calcium Phosphate Coatings on Pure Magnesium. *J. Am. Ceram. Soc.* 102, 123–135. doi:10.1111/jace.15888

Johnston, S., Shi, Z., and Atrens, A. (2015). The Influence of Ph on the Corrosion Rate of High-Purity Mg, Az91 and Ze41 in Bicarbonate Buffered Hanks' Solution. *Corrosion Sci.* 101, 182–192. doi:10.1016/j.corsci.2015.09.018

Johnston, S., Shi, Z., Hoe, C., Uggowitzer, P. J., Cihova, M., Löffler, J. F., et al. (2018). The Influence of Two Common Sterilization Techniques on the Corrosion of Mg and its Alloys for Biomedical Applications. *J. Biomed. Mater. Res. B: Appl. Biomater.* 106, 1907–1917. doi:10.1002/jbm.b.34004

Keim, S., Brunner, J. G., Fabry, B., and Virtanen, S. (2011). Control of Magnesium Corrosion and Biocompatibility with Biomimetic Coatings. *J. Biomed. Mater. Res. Part B: Appl. Biomater.* 96, 84–90. doi:10.1002/jbm.b.31742

Kirkham, G., and Cartmell, S. (2007). Genes and Proteins Involved in the Regulation of Osteogenesis. *Top. Tissue Eng.* 3, 1–22.

Komori, T. (2009). "Regulation of Osteoblast Differentiation by Runx2," in *Osteoimmunology* (Boston: Springer), 43–49. doi:10.1007/978-1-4419-1050-9_5

Lorenz, C., Brunner, J. G., Kollmannsberger, P., Jaafar, L., Fabry, B., and Virtanen, S. (2009). Effect of Surface Pre-Treatments on Biocompatibility of Magnesium. *Acta Biomater.* 5, 2783–2789. doi:10.1016/j.actbio.2009.04.018

Narayanan, R., Seshadri, S., Kwon, T., and Kim, K. (2008). Calcium Phosphate-Based Coatings on Titanium and its Alloys. *J. Biomed. Mater. Res. B: Appl. Biomater. Official J. Soc. Biomater.* 85, 279–299. doi:10.1002/jbm.b.30932

Noviana, D., Paramitha, D., Ulum, M. F., and Hermawan, H. (2016). The Effect of Hydrogen Gas Evolution of Magnesium Implant on the Postimplantation Mortality of Rats. *J. Orthop. Transl.* 5, 9–15. doi:10.1016/j.jot.2015.08.003

Öcal, E. B., Esen, Z., Aydınol, K., and Dericioğlu, A. F. (2020). Comparison of the Short and Long-Term Degradation Behaviors of As-Cast Pure Mg, Az91 and We43 Alloys. *Mater. Chem. Phys.* 241, 122350. doi:10.1016/j.matchemphys.2019.122350

Pichler, K., Kraus, T., Martinelli, E., Sadoghi, P., Musumeci, G., Uggowitzer, P. J., et al. (2014). Cellular Reactions to Biodegradable Magnesium Alloys on Human Growth Plate Chondrocytes and Osteoblasts. *Int. Orthop.* 38, 881–889. doi:10.1007/s00264-013-2163-3

Radha, R., and Sreekanth, D. (2017). Insight of Magnesium Alloys and Composites for Orthopedic Implant Applications - a Review. *J. Magnesium Alloys* 5, 286–312. doi:10.1016/j.jma.2017.08.003

Rahim, M. I., Tavares, A., Evertz, F., Kieke, M., Seitz, J. M., Eifler, R., et al. (2017). Phosphate Conversion Coating Reduces the Degradation Rate and Suppresses Side Effects of Metallic Magnesium Implants in an Animal Model. *J. Biomed. Mater. Res. Part B: Appl. Biomater.* 105, 1622–1635. doi:10.1002/jbm.b.33704

Schumacher, S., Roth, I., Stahl, J., Bäumer, W., and Kietzmann, M. (2014). Biodegradation of Metallic Magnesium Elicits an Inflammatory Response in Primary Nasal Epithelial Cells. *Acta Biomater.* 10, 996–1004. doi:10.1016/j.actbio.2013.10.030

Shadanbaz, S., and Dias, G. J. (2012). Calcium Phosphate Coatings on Magnesium Alloys for Biomedical Applications: A Review. *Acta Biomater.* 8, 20–30. doi:10.1016/j.actbio.2011.10.016

Song, G. (2005). Recent Progress in Corrosion and Protection of Magnesium Alloys. *Adv. Eng. Mater.* 7, 563–586. doi:10.1002/adem.200500013

Song, G. (2007). Control of Biodegradation of Biocompatable Magnesium Alloys. *Corrosion Sci.* 49, 1696–1701. doi:10.1016/j.corsci.2007.01.001

Stachewicz, U., Qiao, T., Rawlinson, S. C., Almeida, F. V., Li, W-Q., Cattell, M., et al. (2015). 3d Imaging of Cell Interactions with Electrospun Plga Nanofiber Membranes for Bone Regeneration. *Acta Biomater.* 27, 88–100. doi:10.1016/j.actbio.2015.09.003

Staiger, M. P., Pietak, A. M., Huadmai, J., and Dias, G. (2006). Magnesium and its Alloys as Orthopedic Biomaterials: A Review. *Biomaterials* 27, 1728–1734. doi:10.1016/j.biomaterials.2005.10.003

Tian, Q., Lin, J., Rivera-Castaneda, L., Tsanhani, A., Dunn, Z. S., Rodriguez, A., et al. (2019). Nano-to-Submicron Hydroxyapatite Coatings for Magnesium-Based Bioresorbable Implants–Deposition, Characterization, Degradation, Mechanical Properties, and Cytocompatibility. *Scientific Rep.* 9, 1–27. doi:10.1038/s41598-018-37123-3

Zai, B. A., Khan, A. S., and Mehboob, H. (2015). Finite Element Method Analysis of a Jaw Structure upon Surgically Assisted Rapid Maxillary Expansion with Various Surgical Procedure. *J. Pak. Dent. Assoc.*, 24 70–74.

Zeller-Plumhoff, B., Gile, M., Priebe, M., Slominska, H., Boll, B., Wiese, B., et al. (2021). Exploring Key Ionic Interactions for Magnesium Degradation in Simulated Body Fluid – a Data-Driven Approach. *Corrosion Sci.* 182, 109272. doi:10.1016/j.corsci.2021.109272

Zou, Y-H., Zeng, R-C., Wang, Q-Z., Liu, L-J., Xu, Q-Q., Wang, C., et al. (2016). Blood Compatibility of Zinc–Calcium Phosphate Conversion Coating on Mg–1.33 Li–0.6 Ca Alloy. *Front. Mater. Sci.* 10, 281–289. doi:10.1007/s11706-016-0345-9

Conflict of Interest: The authors declare that the research was conducted in the absence of any commercial or financial relationships that could be construed as a potential conflict of interest.

Publisher's Note: All claims expressed in this article are solely those of the authors and do not necessarily represent those of their affiliated organizations, or those of the publisher, the editors and the reviewers. Any product that may be evaluated in this article, or claim that may be made by its manufacturer, is not guaranteed or endorsed by the publisher.